**Article:**

Zhang, S. Y., Huang, H., Wu, H. Y. et al. (2026) Conversion electron spectroscopy unveils internal transition pathways of isomers in the neutron-deficient nuclei 179,181Hg and 179Tl. Physical Review C. 014325. ISSN: 2469-9993

https://doi.org/10.1103/ggc8-mn83

# Conversion electron spectroscopy unveils internal transition pathways of isomers in the neutron-deficient nuclei $^{179,181}$Hg and $^{179}$Tl

S. Y. Zhang,[1] H. Huang,[2,3] H. Y. Wu,[4,1] C. Y. Guo,[1] D. W. Luo,[1] L. Ni,[1] Z. H. Li,[1,*] A. N. Andreyev,[5,6,†] Z. Liu,[2,3] H. Hua,[1] D. X. Wang,[1] A. Barzakh,[7] Z. X. Zhou,[1] S. Antalic,[8] B. Andel,[8] A. Sitarčík,[8] J. Z. Zhang,[1] Y. X. Ren,[1] J. Y. Yi,[1] J. F. Wang,[1] W. J. Pan,[1] W. Q. Zhang,[2,3] Q. B. Zeng,[2,3] Z. G. Gan,[2,3] Z. Y. Zhang,[2,3] M. H. Huang,[2,3] H. B. Yang,[2,3] L. Ma,[2,3] J. G. Wang,[2,3] and M. M. Zhang[2,3]

[1]*School of Physics and State Key Laboratory of Nuclear Physics and Technology, Peking University, Beijing 100871, China*
[2]*Institute of Modern Physics, Chinese Academy of Sciences, Lanzhou 730000, China*
[3]*University of Chinese Academy of Sciences, Beijing 100049, China*
[4]*Key Laboratory of Nuclear Data, China Institute of Atomic Energy, Beijing 102413, China*
[5]*School of Physics, Engineering and Technology, University of York, York YO10 5DD, United Kingdom*
[6]*Advanced Science Research Center, Japan Atomic Energy Agency, Tokai-mura, Ibaraki 319-1195, Japan*
[7]*Petersburg Nuclear Physics Institute, NRC Kurchatov Institute, Gatchina 188300, Russia*
[8]*Department of Nuclear Physics and Biophysics, Comenius University in Bratislava, 84248 Bratislava, Slovakia*

(Dated: April 21, 2026)

The isomers in the very neutron-deficient isotopes $^{179m,181m}$Hg and $^{179m}$Tl were populated via fusion-evaporation reaction $^{78}$Kr+$^{107}$Ag $\rightarrow$ $^{185}$Bi$^{*}$. Using the gas-filled recoil separator SHANS, the nuclei of interest were efficiently transported and separated from scattered beam particles and unwanted reaction products. In this study, conversion electrons (CEs) associated with isomeric transitions (ITs) of these isomers were observed for the first time. The CE-$\alpha$ correlation measurements provided crucial insights into their decay properties. For $^{179m}$Tl, a previously unknown IT branch was identified, and a tentative IT decay scheme was proposed. For $^{179m,181m}$Hg, the analysis of CEs served to validate and update their IT decay pathways.

## I. INTRODUCTION

Neutron-deficient nuclei near the proton shell closure at $Z = 82$ exhibit rich structure phenomena, such as shape coexistence and shape evolution, which arise from the interplay between single-particle and collective effects (see e.g. Refs. [1–3] and references therein). Isomers serve as sensitive probes for investigating shape-related phenomena, many of them have been identified in neutron-deficient mercury (Hg, $Z = 80$), and thallium(Tl, $Z = 81$) isotopes [4–18]. In these isotopes, the de-excitation of isomers often involves internal conversion, which is essential for determining the multipolarities of nuclear transition and the configuration of isomeric states, thereby providing key information on nuclear structure. However, detail studied of internal conversion in such nuclei have not been fully explored, largely due to the difficulty of measuring low-energy conversion electrons (CEs). These measurements demand high-efficiency detectors with low energy thresholds, which are often challenged by high background rates adn noise-related triggering issues.

For neutron-deficient $^{179,181}$Hg, $^{179}$Tl isotopes, their isomers have been identified in previous studies [5, 6, 10–12]. The available respective spin-parities, half-lives and decay modes of these isomers are summarized in Table I. However, the de-excitation pathways of these isomers are not yet fully characterized.

In the case of $^{179m}$Hg, the oblate $13/2^{+}$ isomer was identified through $\alpha$-decay study of $^{183}$Pb at RITU gas-filled separator [5]. Its decay to the weakly prolate deformed ground state proceeds via a cascade consisting of an 111-keV $M2$ transition followed by a 61-keV $M1$ transition. The multipolarities of these isomeric transitions (ITs) were inferred by comparing the intensity ratio of $\gamma$ rays and Hg K x-rays with calculated internal conversion coefficient without direct measurement of the CEs [19]. The isomer $^{181m}$Hg was identified following its production via the complete fusion reaction $^{40}$Ca + $^{144}$Sm $\rightarrow$ $^{184}$Pb$^{*}$ at the velocity filter SHIP(GSI)[6]. Its de-excitation was proposed to proceed via an unobserved, strongly converted transition, followed by a newly identified cascade of a 90.3-keV $M1$ and a 71.4-keV $E2$ $\gamma$-ray transition. As in the case of $^{179m}$Hg, the multipolarities of two observed $\gamma$ transitions were assigned based on intensity analyses. The unobserved transition was initially suggested to be an $E3$ transition based on the Weisskopf estimate [6]. However, a recent investigation of $^{183m}$Hg [9] suggested an $M2$ character for this transition instead, by analogy with $^{183m}$Hg. Such assignment implies that the proposed IT cascade cannot reach the $1/2^{-}$ ground state. Thus, the de-excitation path of $^{181m}$Hg requires further investigation.

For $^{179m}$Tl, its $\alpha$-decay chain down to $^{167}$Re has been established in the same experiment at GSI which $^{181m}$Hg was studied [10], yet no $\gamma$ rays or CEs of ITs of $^{179m}$Tl has been detected. Consequently, the excitation energy

* zhli@pku.edu.cn
† andrei.andreyev@york.ac.uk

TABLE I. The spin-parities, half-lives, $\alpha$-decay and IT properties of the isomers denoted as "m" and ground states denoted as "g" in our studied nuclei, respectively. The data are from [5, 6, 10–12], except from the branching ratio of $^{179m}$Tl deduced by the present work.

| nuclide | spin-parity | $T_{1/2}$ (s) | $E_\alpha$ (keV) | $b_\alpha$ (%) | $b_{IT}$(%) | $\gamma$ rays from IT (keV) | reference |
|---|---|---|---|---|---|---|---|
| $^{179m}$Tl | $11/2^-$ | $1.46(4)\times10^{-3}$ | 7207(5) | 75(10) | 25(10) | - | Ref. [10] |
| | | $1.40(3)\times10^{-3}$ | 7206(4) | 75(10) | 25(10) | - | Ref. [12] |
| $^{179g}$Tl | $1/2^+$ | 0.265(10) | 6560(6) | 60(2) | - | - | Ref. [11] |
| $^{179m}$Hg | $13/2^+$ | $6.4(9)\times10^{-6}$ | - | - | 100 | 110.8, 60.6 | Ref. [5] |
| $^{179g}$Hg | $7/2^-$ | 1.050(3) | 6285(3) | 55(25) | - | - | Ref. [5] |
| $^{181m}$Hg | $13/2^+$ | $0.48(2)\times10^{-3}$ | - | - | 100 | 90.3, 71.4 | Ref. [6] |
| $^{181g}$Hg | $1/2^-$ | 3.4(3) | 6006(5) | 24(2) | - | - | Ref. [6] |

of $^{179m}$Tl remains unknown. Within this decay chain, the isomeric states possess the same spin-parity $I^\pi = 11/2^-$ [10, 20–22] and were expected to exhibit similar reduced $\alpha$-decay width. However, the measured value for $^{179m}$Tl is 89(4) keV, which is approximately 30% larger than those of its daughters $^{175m}$Au [67(4) keV] and $^{171m}$Ir [54(7) keV] [10]. This discrepancy suggests the existence of an unobserved decay branch, potentially including proton emission or ITs.

In this work, we report the first observation of CEs associated with ITs in $^{179m,181m}$Hg and $^{179m}$Tl. The measurements for low-energy CEs were performed by employing a digital data acquisition system coupled with pulse-shape analysis techniques, which provides a lower-energy threshold and a significant reduction in background events. For $^{179m}$Tl, the observed correlation CE($^{179m}$Tl)-$\alpha$($^{179g}$Tl) reveals a previously unobserved IT branch. A revised IT decay scheme is proposed and compared with neighboring isotopes. In the case of $^{181m}$Hg, the present CE data, combined with previous $\gamma$-ray measurements [6], allow for identification of a refined decay scheme and an estimation of the isomer's excitation energy. Furthermore, the IT path of $^{179m}$Hg, which was initially established via $\alpha$-decay spectroscopy [5], is corroborated by the present CE measurements.

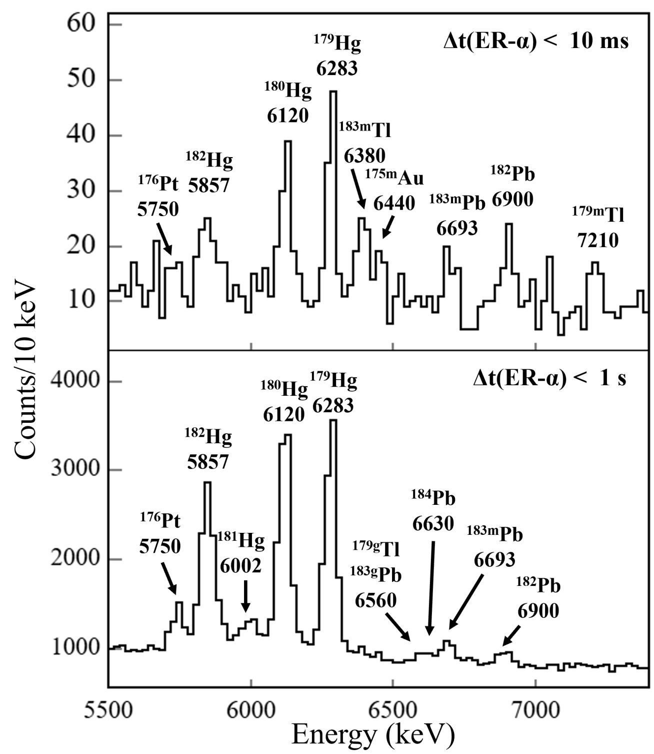


FIG. 1. Energy spectra of ER–$\alpha$ correlations registered in the DSSSD for the reaction $^{78}$Kr+$^{107}$Ag. The spectra are shown for two correlation-time windows, $\Delta t(\mathrm{ER}-\alpha) < 10$ ms (top) and $\Delta t(\mathrm{ER}-\alpha) < 1$ s (bottom). Peaks are labeled by the parent nuclides of the corresponding $\alpha$ decays [23]

.

## II. EXPERIMENT

The nuclei of interest were produced by the fusion-evaporation reaction $^{78}$Kr+$^{107}$Ag $\rightarrow$ $^{185}$Bi*, via different particles evaporation channels: $\alpha 2n$ for $^{179}$Tl, $\alpha pn$ for $^{179}$Hg and $3pn$ for $^{181}$Hg. The $^{78}$Kr beam, with a typical intensity of about 100 pnA and an energy of 353 MeV, was provided by the Sector-Focusing Cyclotron (SFC) of the Heavy Ion Research Facility in Lanzhou (HIRFL), China. An 800 $\mu$g/cm$^2$ $^{107}$Ag target (97.8% enriched) with a 40 $\mu$g/cm$^2$ carbon backing was used. Evaporation residues (ERs) were separated using the SHANS gas-filled recoil separator, which was filled with 0.6 mbar helium gas [24]. After separation, the ERs passed through two multi-wire proportional counters (MWPCs) before being implanted into a 300 $\mu$m thick double-sided silicon strip detector (DSSSD) with 6144 pixels (48 $\times$ 128 strips). The coincidences between signals from the MWPCs and DSSSD were used to distinguish the emitted particles from the implanted ions. The $\gamma$ rays emitted by the implanted ERs or their decay products were measured by four germanium detectors (2 HPGe, 1 Ge-clover

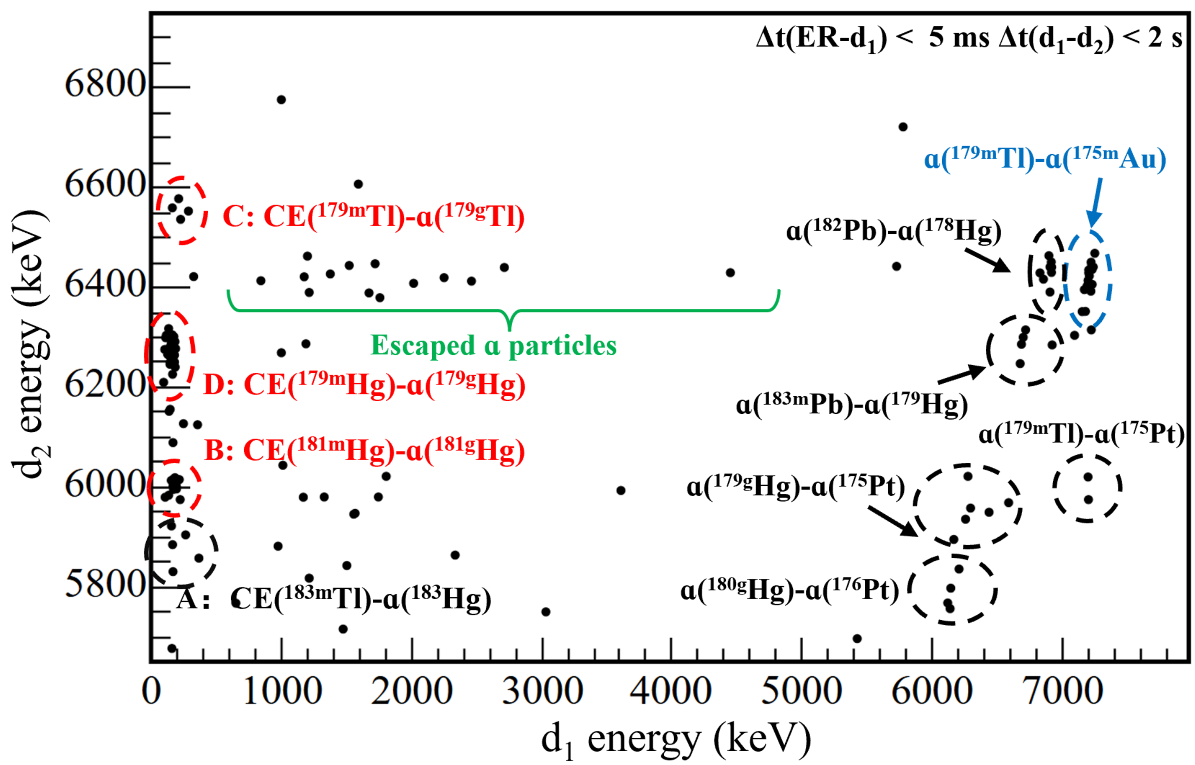


FIG. 2. Two-dimensional $E_{d1}$-$E_{d2}$ plot with $\Delta t(\text{ER-d}_1) < 5$ ms and $\Delta t(\text{d}_1\text{-d}_2) < 2$ s. The time interval are determined based on the half-life of nuclides of interest, $^{179m}$Tl ($\sim$ 1.4ms [10, 12]) for the first generation decay, $^{179g}$Tl (265(10) ms [11]) and $^{175m}$Au (138(5) ms [10]) for the second generation decay, in order to reduce the counting of other strongly populated nuclides and highlight correlation of $^{179m}$Tl.

and 1 LEPS detector) surrounding the DSSSD. More details of this experiment are available in Refs. [25, 26].

The detection signals were recorded by the general-purpose digital data acquisition system (GDDAQ) [27] and analyzed using the CERN ROOT framework [28]. The 16-$\mu$s waveforms from the preamplifiers of the DSSSD were digitized at a sampling rate of 250 MHz. The background resulted from light-charged particles in the $\alpha$ spectrum was effectively reduced by exploiting the distinct pulse-shape characteristics of decay particles and energetic light particles punching through the DSSSD [26].

The $\alpha$-energy calibration of the DSSSD was performed using known $\alpha$-decay lines from $^{166,167}$Os, $^{162,163}$W, $^{158}$Hf and $^{167}$Ir produced in the reaction of $^{78}$Kr+$^{92}$Mo $\rightarrow$ $^{170}$Pt$^*$. The typical energy resolution in the range of 5000–7000 keV is $\sim$ 50 keV (FWHM). The calibration in the low energy range was performed with three CE peaks of $^{183m}$Tl produced in our experiment (see details below), yielding a DSSSD energy resolution of $\sim$25 keV (FWHM) at 300 keV. The energy threshold of DSSSD was at $\sim$ 120 keV.

## III. RESULTS

A part of the $\alpha$-decay spectrum registered in the DSSSD, associated with the decays occurring within 10 ms and 1 s after the implantation of ERs in the same pixel, is shown in Fig. 1, in order to separately present short-lived isomers and the overall population of reaction products. The search for CEs of ITs from isomers to the ground states utilizes a two-dimensional $E_{d1}$-$E_{d2}$ plot, as shown in Fig. 2. (The $d_1$ and $d_2$ refer to the first generation decays from ERs and second generation decays from daughter nuclides.) The time intervals of $\Delta t(\text{ER-d}_1) < 5$ ms and $\Delta t(\text{d}_1\text{-d}_2) < 2$ s are used to highlight the decays of isomers. Some known $\alpha$-$\alpha$ correlations are well identified in the $E_{d1} > 5000$ keV region. In the left side of Fig. 2, four distinct groups are labeled with A–D. The $d_1$ of them are attributed to CEs from ITs and the $d_2$ are the $\alpha$ decays from the ground state of the corresponding nuclide, see Table I. For example, the group C corresponds to the decay chain of $^{181m}$Hg, where $d_1$ corresponds to the CE of $^{181m}$Hg ($\sim$180 keV) and $d_2$ corresponds to $\alpha$ of $^{181g}$Hg (6006 keV). The $\alpha$ particles escaped from DSSSD with partial deposited energy are also seen in Fig. 2. Due to their higher deposited energy $> 1$ MeV, these escaped events will not affect the identification of the CE events

(< 500 keV).

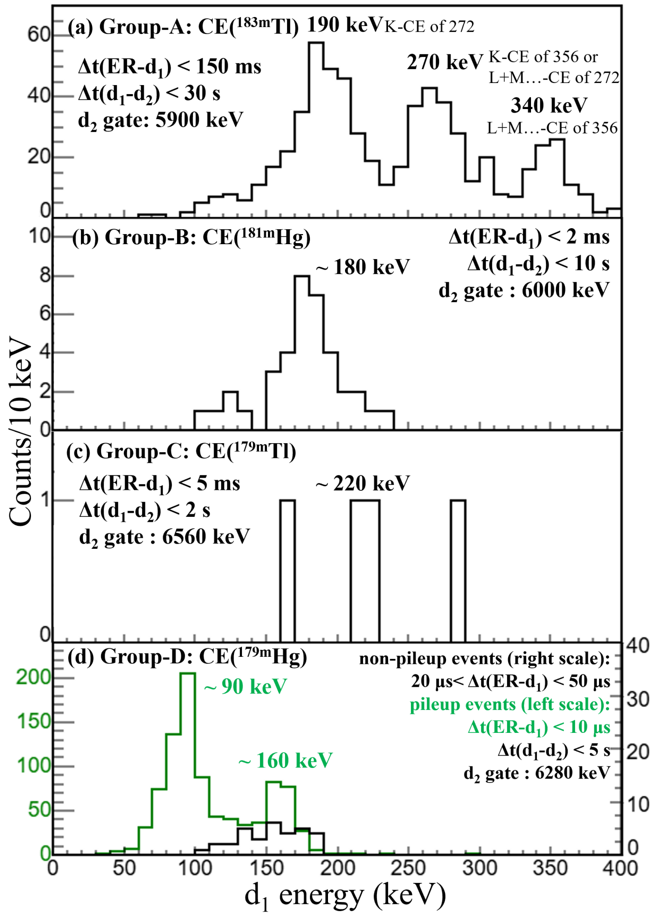


FIG. 3. The CE spectra of (a) $^{183m}$Tl; (b) $^{181m}$Hg; (c) $^{179m}$Tl; (d)$^{179m}$Hg. For (d), the green line represents the CE events reconstructed from pileup data, while black line corresponds to the real-time processed data. They are displayed on different y-axis scales (left for pileup, right for non-pileup) for clarity.

The CE spectra of $^{183m}$Tl, $^{181m}$Hg, $^{179m}$Tl and $^{179m}$Hg are presented in Fig. 3(a), (b), (c), (d), respectively. Unfortunately, for the $\gamma$-ray spectra of the ITs gated on the ground-state $\alpha$ decay for these isomers, only the spectrum of $^{183m}$Tl has sufficient statistics to get reliable information, while the others have limited statistic and do not allow accurate analysis. In the following, we will detail the characteristics of the CE spectra for each group.

**Group A ($^{183m}$Tl):** The IT cascade of $^{183m}$Tl is already known to consist of a 356-keV $E3$ transition followed by a 272-keV $M1$ transition (see Fig. 3 of Ref. [13]). In Fig. 2, Group A exhibits limited statistics due to the short search time $\Delta$t(ER-d$_1$) of 5 ms compared to the known half-life of 53.3(3) ms for $^{183m}$Tl [29]. To increase the statistics, Fig. 3(a) employs a 150 ms time window. Three CE peaks are clearly visible and well correspond to the CEs from different atomic shells as labeled. This good correspondence allows for the energy calibration for low-energy CE range in the present experiment using the known IT energies. A half-life of 53.5(5) ms for $^{183m}$Tl was extracted from an exponential decay fit to the decay-time curve, which shows consistency with the reported value in Ref. [30]. Further details on the coincident CE – $\gamma$ analysis for $^{183m}$Tl can be found in Ref. [26].

**Group B ($^{181m}$Hg):** As shown in Fig. 3(b), the correlation CE spectrum for $^{181m}$Hg is characterized by a single peak at approximately 180 keV in Fig. 3(b). Its half-life is deduced to be 0.50(9) ms, in agreement with the reported value of 0.48(2) ms [6]. This result provides the first direct evidence for the correlation between $^{181m}$Hg and $^{181g}$Hg.

**Group C ($^{179m}$Tl):** The four CE events in Fig. 3(c) represent the first observation of the IT branch in $^{179m}$Tl. The half-life of $^{179m}$Tl is deduced to be 1.3(6) ms using a maximum likelihood method [31], in agreement with the reported value of $\sim$ 1.4 ms [10, 12]. Additionally, the known $\alpha$ decays from $^{179m}$Tl to $^{175m}$Au are also observed in our experiment, as shown in Fig. 2, with 18 counts in total.

**Group C ($^{179m}$Tl):** The four CE events in Fig. 3(c) represent the first observation of the IT branch in $^{179m}$Tl. The half-life of $^{179m}$Tl is deduced to be 1.3(6) ms using a maximum likelihood method [31], in agreement with the reported value of $\sim$1.4 ms [10, 12]. The half-life and decay energy of the second-generation decay in this cluster are deduced to be $0.5^{+0.5}_{-0.2}$ s and 6563(19) keV, respectively. It should be noted that, as shown in Fig. 1, the $\alpha$ line around 6560 keV observed in the present experiment may also contain a contribution from the $\alpha$ decay of $^{183g}$Pb feeding the $3/2^-$ state in $^{179}$Hg ($E_\alpha = 6570(10)$ keV, $T_{1/2} = 535(30)$ ms, branching ratio = 28(4)% [5]), which is also consistent with the second-generation decay observed here. Therefore, these CE events could also originate from a previously unknown ms-isomer in $^{183}$Pb decaying to the $3/2^-$ state in $^{179}$Hg. However, this possibility can be firmly excluded by the present data. If such an isomer existed in $^{183}$Pb, CE events should also appear in coincidence with the another 6775 keV $\alpha$ branch of $^{183g}$Pb, with about 10 counts expected based on its branching ratio = 72(5)%, whereas no such events are observed. In addition, the known $\alpha$ decays from $^{179m}$Tl to $^{175m}$Au are also seen in our experiment, as shown in Fig. 2, with 18 counts in total, which allows a subsequent determination of the branching ratio.

**Group D ($^{179m}$Hg):** Due to the shorter half-life of $^{179m}$Hg (6.4 $\mu$s [5]) compared to the dead time of DAQ (20 $\mu$s [26]), most decay events associated with $^{179m}$Hg would not be recorded following the implantation. However, the pulse shape of the implantation signal was captured in this experiment. The fast-decaying pulses pile up on the implantation pulse shape, and can be reconstructed using the digital pileup pulse processing method. The processing detail can be found in Refs.

[7, 26, 32–35]. The CE spectrum reconstructed from the pileup pulses is shown in Fig. 3(d) with the green line, while the CE spectrum processed in real time on GDDAQ is drawn with black line. Both CE spectra exhibit a peak around 160 keV, but the 90-keV CE peak is absent in non-pileup spectrum. This difference can be attributed to the lower energy threshold of the pileup pulse data (∼ 70 keV), compared to the non-pileup data from GDDAQ (∼ 120 keV). In the experiment, the signal trigger threshold was set slightly above the noise level. In contrast, the offline analysis for pileup pulse reconstruction was not constrained by this threshold, because GDDAQ was triggered by the pulse of ER implantation. The subsequent CE signal was then reconstructed by the digital pileup pulse processing method [32], which effectively distinguished the small pulses down to 70 keV. As a result, only pile-up data are used for $^{179m}$Hg in the next section.

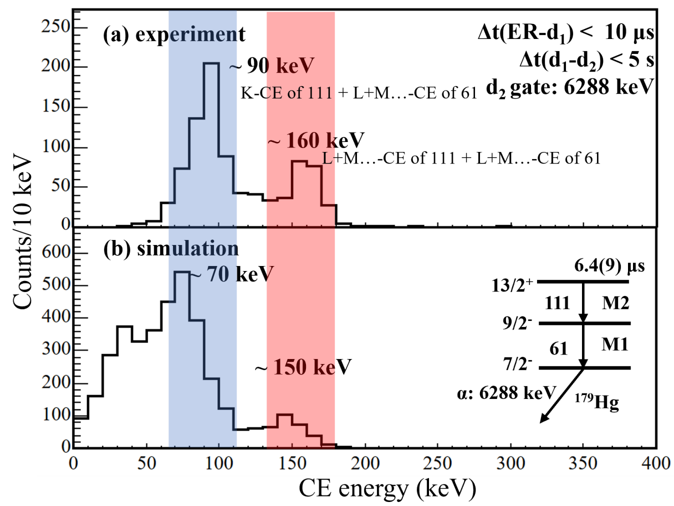


FIG. 4. The comparison between (a) the experimental CE spectrum only using the pileup data and (b) the simulated spectrum of $^{179m}$Hg, based on the IT decay scheme presented on the right-side. The red and blue shadows show the consistency of simulated and experimental CE peaks.

## IV. DISCUSSION

### A. The IT decay of $^{179m}$Hg

The previously reported IT decay scheme of $^{179m}$Hg [5] is shown in the inset of Fig. 4(b). Since each IT transition can generate CEs from different electron shells, multiple peaks are expected to appear in the CE spectrum. Here, they are mainly classified into two types, K-CE and L+M...-CE, according to their energies. As labeled in Fig. 4(a), the 90-keV peak originates from the summing of L+M+..-CE from the $M1$ 61-keV decay and K-CE from $M2$ 111-keV decay, while 160-keV peak represents the summing of L+M+..-CE from the $M1$ 61-keV decay and L+M+..-CE from the $M2$ 111-keV decay.

To better understand this scenario, Geant4 Monte Carlo simulations were performed [26, 36]. In the simulation, the emission probabilities for CEs were provided by the conversion coefficients calculated by BrIcc [37]. The simulated result is presented in Fig. 4(b), which reproduces the experimental data well. A minor deviation is observed for the 90 keV peak, which is likely attributable to the energy threshold ∼ 70 keV applied in processing pileup data.

Based on the present data, the experimental $K/L$ conversion ratio of the 111 keV transition is deduced to be $\alpha_K(111\text{ keV})/\alpha_L(111\text{ keV}) = 1.5(2)$. This value should be regarded as a lower limit rather than an absolute one, since the low-energy peak around 90 keV is affected by the above-mentioned threshold effect and some counts may therefore be lost. The experimental value is close to the BrIcc-calculated ratio $\alpha_K/\alpha_L(111\text{ keV}, M2) = 2.69(6)$. For comparison, the corresponding ratios calculated by BrIcc for other possible multipolarities of the 111 keV transition are 0.247 ($E2$), 0.0165 ($E3$) and 0.506 ($M3$), all of which are significantly smaller than the experimental lower limit and can therefore be excluded. The $E1$ and $M1$ multipolarities are also clearly ruled out, since their Weisskopf single-particle estimates yield partial half-lives of about $2 \times 10^{-3}$ ns and 0.1 ns, respectively, much shorter than the observed 6.4 $\mu$s half-life of $^{179m}$Hg. Therefore, our data independently support an $M2$ assignment for the 111 keV transition, in agreement with the decay scheme proposed in Ref. [5].

### B. The IT decay of $^{181m}$Hg

An isomer in $^{181}$Hg with spin-parity $13/2^+$ and a half-life of 0.48 ms was previously identified in an experiment utilizing the SHIP separator [6]. Its IT decay was determined as a cascade consisting of $\Delta E_1$ − 90.3-keV($M1$) − 71.4-keV($E2$) transitions, based on the $\gamma$-ray and Hg X-ray spectroscopic analysis. In ref. [6], an unobserved, highly converted transition $\Delta E_1$ keV was suggested to have an $E3$ character to explain the isomeric decay. However, a recent study reinterprets its multipolarity as $M2$ by analogy with $^{183m}$Hg [9]. Consequently, the de-excitation path of $^{181m}$Hg changes from $13/2^+ \to 7/2^- \to 5/2^-$ to $13/2^+ \to 9/2^- \to 7/2^-$. In this scenario, the 90.3 keV $M1$ transition observed in Ref. [6] likely corresponds to the decay from the known $9/2^-$ state at x + 91 keV to the $7/2^-$ state at x keV with the $5/2^-[512]$ configuration [7]. Due to the $E2$ multipolarity, the subsequent 71.4-keV transition, however, cannot reach the $1/2^-$ ground state.

In the present work, the observed CEs of $^{181m}$Hg confirm the connection between $^{181m}$Hg and $^{181g}$Hg. To con-

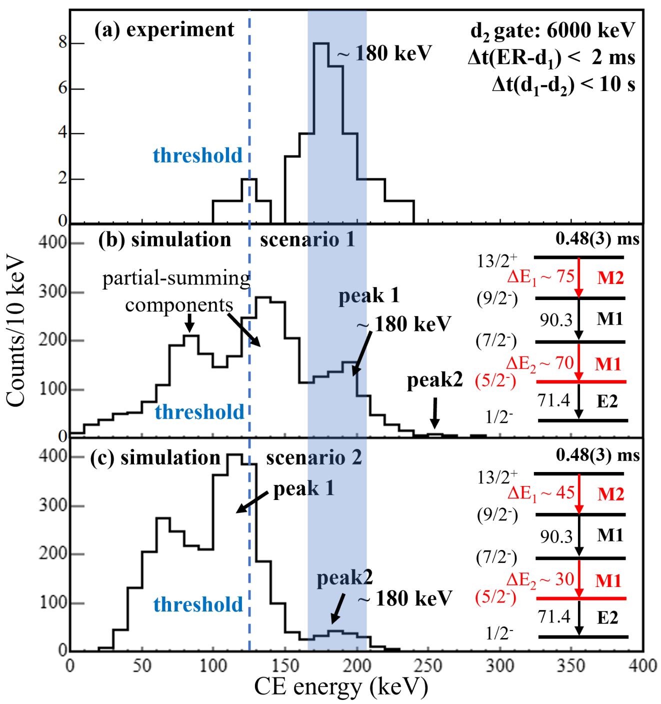


FIG. 5. The comparison between the experimental CE spectrum of $^{181m}$Hg (a) and the simulated spectra based on two representative IT decay schemes: scenario 1 with $\Delta E_1 \sim 75$ keV, $\Delta E_2 \sim 70$ keV (b), and scenario 2 with $\Delta E_1 \sim 45$ keV, $\Delta E_2 \sim 30$ keV (c). In the simulations, peak 1 corresponds to the summed conversion-electron events involving the K-shell electrons of the 90.3-keV transition, while peak 2 arises from the sum of L+M...CEs. The low-energy structure visible below peak 1 originates from partial-summing events,which occur when one or more transitions in the cascade proceed via $\gamma$-ray emission rather than via internal conversion.

struct the complete IT decay cascade from $^{181m}$Hg to $^{181g}$Hg, an additional unobserved transition $\Delta E_2$ keV is proposed, as shown in the inset of Fig. 5(b). The ordering of $\Delta E_2$ and 71.4-keV transitions will be addressed below.

In Ref. [6], an upper energy limit of $B_e(K) = 83$ keV (K-electron binding energy in Hg [38]) was estimated for $\Delta E_1$, as in this IT cascade, only 90.3-keV transition has K x-rays, which was supported by the coincident gamma spectra (see Fig. 1 of Ref. [6]). For the same reason, namely the absence of K x-rays, $\Delta E_2$ also cannot exceed 83 keV.

The CE energy peak of $^{181m}$Hg around 180 keV shown in Fig. 5(a), can be attributed to the summation of the CEs from these IT transitions. The analysis follows the procedure similar to that for $^{179m}$Hg. The 90.3 keV transition has both K-CEs and L+M+..-CEs, whereas $\Delta E_1$, $\Delta E_2$ and 71.4 keV transitions possess only L+M+..-CEs, since their energies are lower than $B_e(K)$. Under ideal conditions with the sufficiently-low CE energy threshold, two distinct summing peaks (denoted as peak 1 and peak 2) would be present in the CE spectrum of $^{181m}$Hg as shown in Fig. 5(b). Peak 1 is associated with the summation of K-CE of 90.3 keV transition and L+M+..CEs from $\Delta E_1$, $\Delta E_2$ and 71.4 keV transitions, while the peak 2 arises solely from the summation of their L+M+..CEs. However, in Fig. 5(a), only a single CE peak is observed, suggesting two possible explanations.

In the scenario 1, assuming the observed peak in Fig. 5(a) is peak 1, the sum $\Delta E_1 + \Delta E_2$ should be $\sim 145$ keV, and both $\Delta E_1$ and $\Delta E_2$ should lie within 62-83 keV by the upper limit of 83 keV discussed above. In this case, the non-observation of peak 2 in the present CE spectrum can be understood. Based on the BrIcc-calculated $\alpha_K/\alpha_L$ ratio for the 90.1-keV transition [37], the expected contribution of peak 2 around 220 keV would be only about three counts, which could be obscured by the right-tail of the observed peak 1. However, an additional constraint comes from the previously reported $\gamma$-ray data in Ref. [6]. For the above energy range, BrIcc gives $\alpha_{\rm tot}^{\rm cal}(\Delta E_1, M2) = 50$–$250$ and $\alpha_{\rm tot}^{\rm cal}(\Delta E_2, M1) = 2.5$–$7.0$, respectively [37]. These values can be compared with the experimentally deduced conversion coefficients of the 71.4-keV and 90.3-keV transitions reported in Ref. [6], namely $\alpha_{\rm tot}^{\rm exp}(71.4\ {\rm keV}) = 19(4)$ and $\alpha_K^{\rm exp}(90.3\ {\rm keV}) = 7.3$. Therefore, the inferred $\Delta E_2$ transition would have a smaller conversion coefficient and hence a relatively stronger $\gamma$-ray branch. It should therefore be at least as observable in the $\gamma$-ray spectrum as the 71.4-keV and 90.3-keV transitions. However, in Fig. 1 of Ref. [6], the 71.4-keV and 90.3-keV $\gamma$ rays were observed, whereas no evidence for $\Delta E_2$ was reported. For this reason, Scenario 1 is considered less favored.

In the scenario 2, where the observed CE peak represents peak 2, the sum $\Delta E_1 + \Delta E_2$ would be $\sim 75$ keV. In this case, the absence of the peak 1 expected at $\sim 110$ keV is attributed to the energy threshold around 120 keV. Similarly, the calculated ranges of $\alpha_{tot}^{cal}(\Delta E_1, M2)$ and $\alpha_{tot}^{cal}(\Delta E_2, M1)$ are $10^2 - 10^6$ and $10 - 300$, respectively. The analysis reveals that, in contrast to the first scenario, a subset of ($\Delta E_1$, $\Delta E_2$) pairs can satisfy $\alpha_{tot} > 19$. This pattern sets an upper limit of 40 keV for $\Delta E_2$, which provides a basis for discussing the order of $\Delta E_2$ and 71.4-keV transitions. A possible cascade of $\Delta E_1$–90.3 keV–71.4 keV–$\Delta E_2$ would require the presence of a $3/2^-$ state at $\Delta E_2$ keV in $^{181}$Hg. However, due to the 40 keV upper limit for $\Delta E_2$, this state cannot be explained as one of the known $3/2^-$ states at 64 or 269 keV, which were identified in the $\alpha$ decay of $^{185}$Pb [39]. Since no additional $3/2^-$ state at such low energy was populated in that $\alpha$ decay study [39], the most likely ordering of the transitions deexciting from $^{181m}$Hg to $^{181g}$Hg is $\Delta E_1$–90.3 keV–$\Delta E_2$–71.4 keV, as shown in the inset of Fig. 5(b).

Geant4 simulations were performed for both scenarios, and representative simulated CE spectra with $\Delta E_1 = 75$ keV and $\Delta E_2 = 70$ keV (scenario 1) or $\Delta E_1 = 45$ keV and

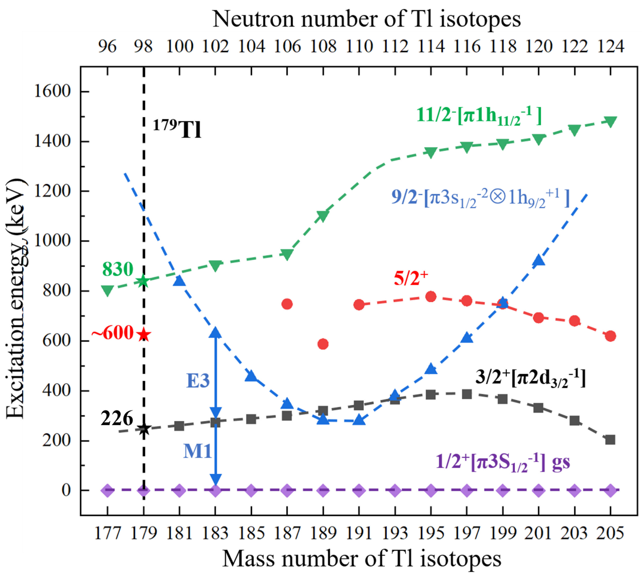


FIG. 6. Experimental excitation energies of selected excited $3/2^+$, $5/2^+$, $9/2^-$ and $11/2^-$ states in odd-$A$ Tl isotopes, relative to the respective $1/2^+$ ground states. Data are taken from Refs. [30, 40–45]. Points marked with star symbols represent the estimated excitation energies for $^{179}$Tl, except that the value of 226 keV is adopted from Ref. [12]. The tentative $9/2^-$ isomer reported in Ref. [12] is not shown, see text for details. The experimental uncertainties are usually smaller than the symbol sizes and therefore not shown. The lines connecting the data points are drawn to guide the eye.

$\Delta E_2$ = 30 keV (scenario 2) are presented in Fig. 5 (b) and (c), respectively. As anticipated, in scenario 1 the observed peak corresponds to peak 1 which is dominated by the K-conversion component of 90.3-keV transition, while peak 2 which is associated with the L+M... CEs of 90.3-keV, would have much lower statistics. However, the simulation for scenario 1 also predicts additional structures around ∼ 80 keV and ∼ 140 keV. These features arise from low-energy partial-summing CE events that occur when one or more transitions proceed via $\gamma$-ray emission rather than CEs. The absence of such structures in the experimental spectru further disfavors scenario 1. In scenario 2 where the observed peak corresponds to peak 2, the simulated spectrum shows reasonable agreement with the observed spectrum, whereas peak 1 and the low-energy partial-summing CE events are suppressed in the measured spectrum due to the ∼120-keV threshold. In these simulations, the positions of peak 1 and peak 2 remain invariant under different allocations of $\Delta E_1$ and $\Delta E_2$. Although the low-energy partial-summing component may shift, it always lies below peak 1 and is therefore unrelated to the observed peak. Based on the above analysis, the sum $\Delta E_1$+$\Delta E_2$ can be confirmed as ∼ 75 keV, and the excitation energy of the $13/2^+$ isomeric state can be deduced to be ∼ 240(40) keV. This uncertainty of 40 keV is dominated by counting-statistics uncertainty and the DSSSD energy resolution.

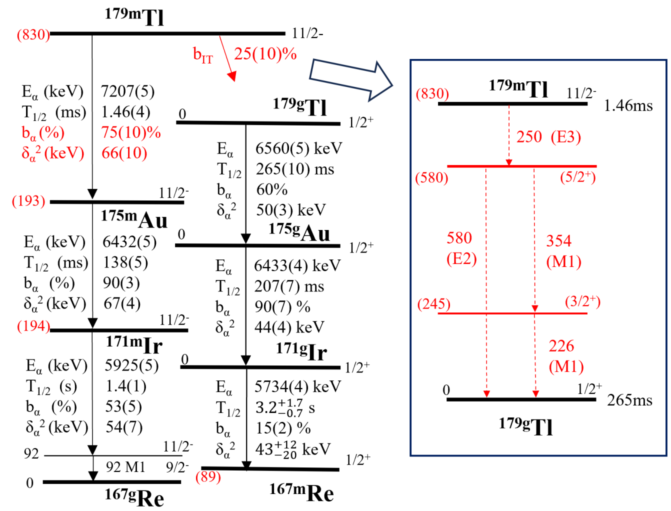


FIG. 7. The IT-decay scheme of $^{179m}$Tl and $\alpha$-decay schemes of $^{179m,g}$Tl and their daughter nuclides. The values shown in red are deduced in present work, except for the 226-keV transition energy of the $3/2^+ \rightarrow 1/2^+$ decay, which is adopted from Ref. [12]. Other values are taken from Refs. [10, 11]. Shown are $\alpha$-decay energies $E_\alpha$, half-life values, $T_{1/2}$, $\alpha$ branching ratios $b_\alpha$, and reduced $\alpha$-decay widths $\delta^2_\alpha$. The reduced $\alpha$-decay widths were calculated with the Rasmussen prescription by assuming $\Delta L = 0$ transitions [46]

### C. The IT decay of $^{179m}$Tl

The low-lying $11/2^-$ isomer in $^{179}$Tl, previously known to decay only via $\alpha$ decay [10–12], is suggested to undergo an IT branch based on the CEs observed in this work. After considering the count ratio of detected $\alpha$ particles and CEs from the decay of $^{179m}$Tl, the $\alpha$-decay branching ratio $b_\alpha = 75(10)\%$ and IT branching ratio $b_{IT} = 25(10)\%$ are obtained, respectively.

$^{179}$Tl has an unpaired proton hole, which can occupy the $3s_{1/2}$, $2d_{3/2}$ or $1h_{11/2}$ orbits below the $Z = 82$ shell gap [47]. The known excitation energies of the $3/2^+$, $9/2^-$, $11/2^-$ excited states in odd-$A$ $^{177-205}$Tl isotopes are shown in Fig. 6 with data taken from [30, 40–45, 48–52]. The excitation energy of the $11/2^-$ isomer in $^{179m}$Tl is interpolated to be about 830 keV [11] based on systematics. The energies of intruder $9/2^-$ states exhibit a pronounced parabolic trend. In the nearby isotopes $^{181,183,185}$Tl, $9/2^-$ intruder states are isomeric and de-excite through a cascade of $9/2^-(E3) \rightarrow 3/2^+(M1) \rightarrow 1/2^+$ [30, 40, 48]. If this intruder $9/2^-$ state also exists in $^{179}$Tl, its expected en-

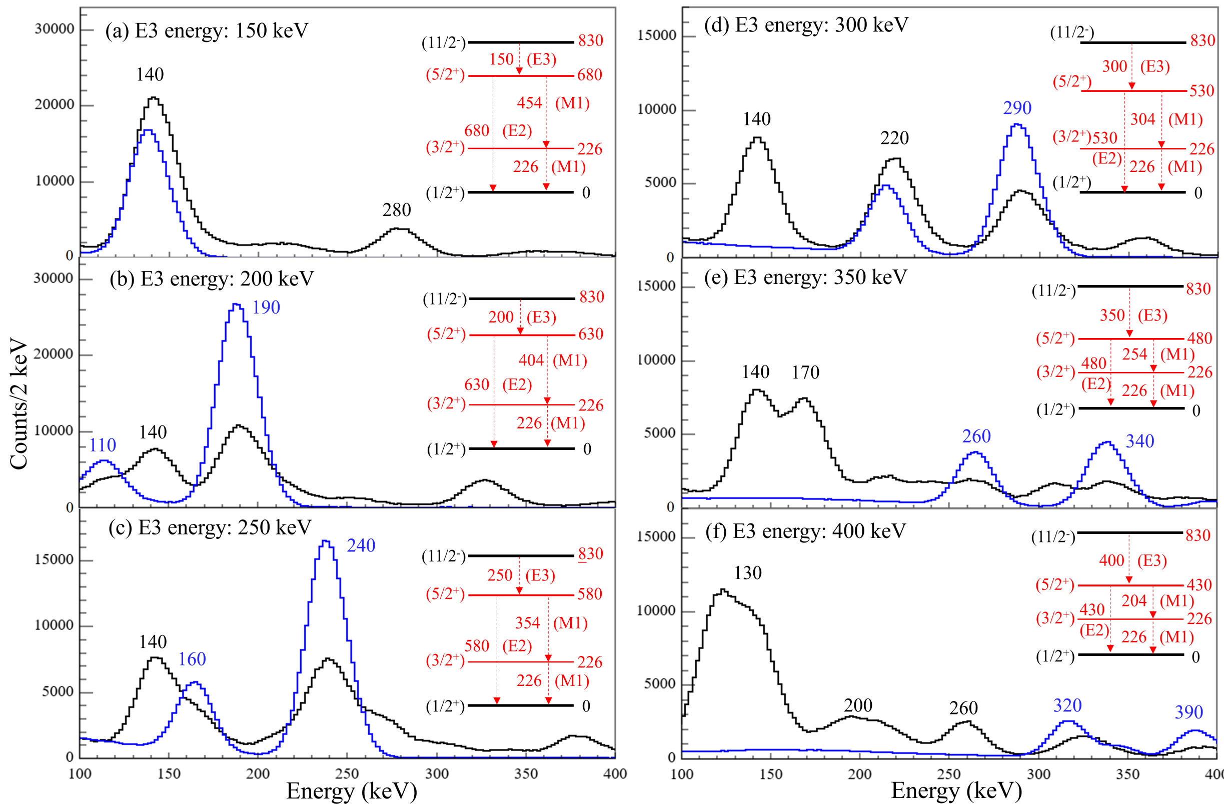


FIG. 8. The results of Geant4 simulations of possible deexcitation paths of $^{179m}$Tl with different $5/2^+$ state. The simulations for the $E3$-$M1$-$M1$ cascade are shown in black, while for the $E3$-$E2$ cascade are shown in blue. The energy threshold is approximate 120 keV and the simulation spectra lower than it are not shown on the plot.

ergy based on the systematic trend would be higher than that of the $11/2^-$ isomer. In this case, a fast $M1$ transition to the $11/2^-$ state could occur, resulting in a relatively short lifetime for the $9/2^-$ state. This level ordering would provide a natural explanation for the existence of the long-lived $11/2^-$ isomer in $^{179}$Tl.

A previous study at the RITU separator reported the observation of a short-lived isomer in $^{179}$Tl with a half-life of $114^{+18}_{-10}$ ns [12]. Three $\gamma$ rays at 94, 584, and 226 keV were observed but without $\gamma$-$\gamma$ coincidence information. The authors tentatively placed these transitions in a cascade, yielding a proposed excitation energy of 904 keV and a $9/2^-$ intruder assignment for this isomer. It should be noted that this excitation energy appears lower than the value of ∼1100 keV expected from the parabolic extrapolation of the $9/2^-$ systematics shown in Fig. 6. A possible explanation could be that a weak $\gamma$-ray transition was missed in the analysis of Ref. [12] due to limited statistics. It is also worth noting that although good statistics for $^{179m}$Tl was obtained in that work, the $\gamma$-ray search was performed within a 1 $\mu$s time window after implantation, which strongly suppresses the detection of the ∼1.4 ms IT decay reported in our work. Nevertheless, assuming that the 226-keV transition corresponds to the low-lying $3/2^+ \rightarrow 1/2^+$ decay as proposed in Ref. [12] , we adopt $E(3/2^+) = 226$ keV in the following discussion and in the Geant4 simulations.

The direct $E5$ transition between the $11/2^-$ isomer and the $1/2^+$ ground state would be extremely hindered, thus, a cascade involving at least two $\gamma$ transitions is expected to connect these states. The observed CE events around 220 keV in Fig. 2 represent the summed transition energy of such cascade. However, due to the low statistics, no $\gamma$ rays from $^{179m}$Tl were measured by the HPGe and Clover detectors in this experiment. Therefore, the detailed IT decay scheme and the excitation energies of the intermediate states in the decay path cannot be firmly established. Nevertheless, a plausible decay scenario can be inferred based on systematics and Geant4 simulations, as explained below.

With E($11/2^-$) ≈ 830 keV and E($3/2^+$) = 226 keV, a direct $M4$ decay from the $11/2^-$ state to the $3/2^+$ state, with an energy of 830 - 226 = 604 keV, would correspond to a Weisskopf-estimated half-life of ∼ 400 s [38], which is incompatible with the reported value of ∼ 1.4 ms in Ref. [10, 12]. This discrepancy implies the existence of an intermediate excited state between the $11/2^-$ and $3/2^+$ states. A plausible candidate is the $5/2^+$ state, which is observed in the heavier odd-$A$ Tl isotopes shown in Fig. 6. In this scenario, the $11/2^-$ state decays to the $5/2^+$

state via an $E3$ transition and then proceeds to the $1/2^+$ ground state either through a single $E2$ transition or via a cascade of $M1$ transitions, i.e. $5/2^+ \rightarrow 3/2^+ \rightarrow 1/2^+$, as shown in Fig. 7.

Due to the scarcity of experimental data on the $5/2^+$ states in neutron-deficient Tl isotopes, systematics can only provide a rough range for the excitation energy of the presumed $5/2^+$ state in $^{179}$Tl. The likely energy of $5/2^+$ state can be further inferred through Geant4 simulation. As shown in Fig. 8, Geant4 simulations of the CE spectra were performed for different energies of $5/2^+$ state, and the $11/2^-$ and $3/2^+$ energies were fixed to 830 keV and 226 keV, respectively. The corresponding de-excitation E3 transition was likely in the range of 150–400 keV, which is agree with the Weisskopf estimate for the $\sim$ 1.4 ms half-life of $^{179m}$Tl [38]. Fig. 8 shows the simulated CE spectra with E3 transition energies in increments of 50 keV. The conversion coefficients ($\alpha_{total}$, $\alpha_K$, $\alpha_L$...) calculated by BrIcc [37] were adopted in the simulations. The simulated CE spectra for the $E3$–$M1$–$M1$ and the $E3$–$E2$ de-excitation branches are shown in black and blue curves, respectively. The comparison with the experimental CE spectrum of $^{179m}$Tl in Fig. 3(c) reveals that only the simulations performed in Fig. 8(b)–(d) which account for the mixture of two de-excitation pathways, can match the observation. By contrast, the predict peaks by other de-excitation scenarios are absent in the present experiment. Therefore, based on above analysis, the energy of $E3$ transition is estimated to be in the range of 200–300 keV, implying the E($5/2^+$) $\approx$ 530–630 keV.

In previous study [11], the reduced $\alpha$-decay width $\delta^2_\alpha$ for the $\alpha$ decay from $^{179m}$Tl was reported as 89(4) keV, significantly higher than those of the daughter nuclides $^{175m}$Au and $^{171m}$Ir, which were reported to be 67(4) keV and 54(7) keV, respectively. This discrepancy was puzzling because the $\delta^2_\alpha$ values for these nuclei, which all involve $\alpha$ decays between $11/2^-$ states with similar configurations, are expected to be comparable. In the present work, we redetermined the $\delta^2_\alpha$ for $^{179m}$Tl to be 66(10) keV. This result was derived using the $\alpha$-decay energy of 7207(5) keV, the reported half-life of $\sim$ 1.4 ms [11, 12], and the newly-determined $\alpha$-decay branching ratio, with the Rasmussen approach assuming $\Delta L = 0$ transition [46] and including screening correction. The revised value of 66(10) keV demonstrates the consistency within the decay chain, thereby resolving the long-standing puzzle of an anomalously high reduced width previously reported in Ref. [10] and providing further support for the presence of the IT branch in $^{179m}$Tl.

Based on the deduced IT branching ratio and the reported half-life of $\sim$ 1.4 ms for $^{179m}$Tl [11, 12], the Weisskopf single-particle transition probability B($E3$) was deduced to be in 0.31 – 1.8 W.u. [38], corresponding to a de-excitation $E3$ transition energy between 200 and 300 keV, as shown in Fig. 9. This obtained B($E3$) value is different from the systematic values of 0.01 – 0.02 W.u. observed in neighboring odd-$A$ isotopes $^{181,183,195-201}$Tl,

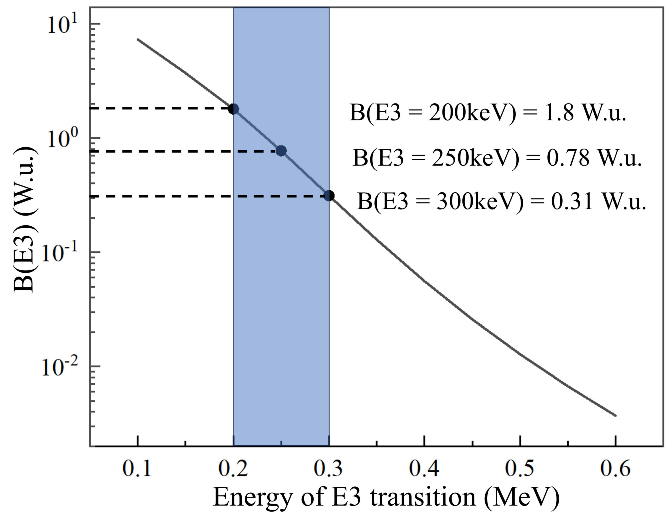


FIG. 9. The relationship of B($E3$) values relative to the $E3$ transition energy of $^{179m}$Tl, calculated using energy and the IT branching ratio deduced in this study along with the lifetime from Ref. [10, 12]. The blue shaded region represents the proposed range of $E3$ transition energy as suggested by the Geant4 simulation.

as the configuration of $^{179m}$Tl is inferred to be $h^{-1}_{11/2}$ rather than intruder $h_{9/2}$ configuration. Further experiment with higher statistics and simultaneous measurement for CEs and $\gamma$ rays are required to clarify the nuclear structure of $^{179m}$Tl.

## V. CONCLUSIONS

We investigated the isomeric states in the neutron-deficient nuclei $^{179,181}$Hg and $^{179}$Tl and their IT decays. These nuclei were produced by the $^{78}$Kr+$^{107}$Ag fusion-evaporation reaction at the gas-filled separator SHANS. The first observation of their CEs provided critical insights into IT de-excitation pathways. For $^{179m}$Hg, the experimental CE spectrum aligned with Geant4 simulations, validated its previously reported IT decay path. In $^{181m}$Hg, the combined analysis of CEs and prior $\gamma$-ray data enabled an updated decay cascade, yielding a determination of the excitation energy of the $13/2^+$ isomer. For $^{179m}$Tl, the newly detected CEs confirmed the existence of a previously unobserved IT branch. A tentative IT decay scheme of $^{179m}$Tl was proposed based on experimental systematics and Geant4 simulations.

## ACKNOWLEDGMENTS

The authors would like to thank Prof. C. F. Jiao for helpful discussion about $^{179m}$Tl. This work was supported by the National Key R&D Program of China (Grant No. 2022YFA1602302), the National Natural Science Foundation of China (Grants No. 12535008, No. 12035001, No. U2167201, No. 12135004, No. 12405140). A.N.A. is grateful for financial support from the UK STFC and the Chinese Academy of Sciences President's International Fellowship Initiative (Grant No. 2026PVA0208). S. A., B. A. and A. S. acknowledge support by the Slovak Research and Development Agency (Contract No. APVV-22-0282) and by the Slovak grant agency VEGA (Contract No. 1/0019/25).

[1] J. G. Cubiss, A. N. Andreyev, A. E. Barzakh, P. Van Duppen, S. Hilaire, S. Péru, S. Goriely, M. Al Monthery, N. A. Althubiti, B. Andel, *et al.*, Phys. Rev. Lett. **131**, 202501 (2023).

[2] P. E. Garrett, M. Zielińska, E. Clément, *et al.*, Prog. Part. Nucl. Phys. **124**, 103931 (2022).

[3] B. A. Marsh, T. Day Goodacre, S. Sels, Y. Tsunoda, B. Andel, A. N. Andreyev, N. A. Althubiti, D. Atanasov, A. E. Barzakh, J. Billowes, *et al.*, Nat. Phys. **14**, 1163 (2018).

[4] F. Kondev, M. Carpenter, R. Janssens, C. Lister, K. Abu Saleem, I. Ahmad, H. Amro, J. Caggiano, C. Davids, A. Heinz, B. Herskind, T. Khoo, T. Lauritsen, W. Ma, J. Ressler, W. Reviol, L. Riedinger, D. Sarantites, D. Seweryniak, S. Siem, A. Sonzogni, P. Varmette, and I. Wiedenhöver, Phys. Lett. B **528**, 221 (2002).

[5] D. G. Jenkins, A. N. Andreyev, R. D. Page, M. P. Carpenter, R. V. F. Janssens, C. J. Lister, F. G. Kondev, T. Enqvist, P. T. Greenlees, P. M. Jones, *et al.*, Phys. Rev. C **66**, 011301 (2002).

[6] A. N. Andreyev, S. Antalic, D. Ackermann, T. E. Cocolios, V. F. Comas, J. Elseviers, S. Franchoo, S. Heinz, J. A. Heredia, F. P. Heßberger, *et al.*, Phys. Rev. C **80**, 044334 (2009).

[7] P. G. Varmette, D. T. Shidot, W. C. Ma, A. V. Ramayya, R. V. F. Janssens, C. N. Davids, J. H. Hamilton, I. Ahmad, H. Amro, B. R. S. Babu, *et al.*, Phys. Lett. B **410**, 103 (1997).

[8] K. Bindra, A. Ramayya, W. Ma, B. Babu, J. Hamilton, L. Chaturvedi, J. Kormicki, R. Janssens, C. Davids, I. Ahmad, *et al.*, Phys. Lett. B **318**, 41 (1993).

[9] H. Huang, W. Q. Zhang, A. N. Andreyev, Z. Liu, D. Seweryniak, Z. H. Li, C. Y. Guo, A. E. Barzakh, P. V. Duppen, B. Andel, *et al.*, Phys. Lett. B **833**, 137345 (2022).

[10] A. N. Andreyev, S. Antalic, D. Ackermann, T. E. Cocolios, V. F. Comas, J. Elseviers, S. Franchoo, S. Heinz, J. A. Heredia, F. P. Heßberger, *et al.*, J. Phys. G **37**, 035102 (2010).

[11] A. N. Andreyev, V. Liberati, S. Antalic, D. Ackermann, A. Barzakh, N. Bree, T. E. Cocolios, J. Diriken, J. Elseviers, D. Fedorov, *et al.*, Phys. Rev. C **87**, 054311 (2013).

[12] H. Badran, C. Scholey, J. Uusitalo, K. Auranen, T. Grahn, P. T. Greenlees, A. Herzáň, U. Jakobsson, R. Julin, S. Juutinen, *et al.*, Phys. Rev. C **96**, 064314 (2017).

[13] M. Venhart, A. N. Andreyev, J. G. Cubiss, J. L. Wood, A. E. Barzakh, C. Van Beveren, T. E. Cocolios, R. P. de Groote, D. V. Fedorov, V. N. Fedosseev, *et al.*, Phys. Rev. C **105**, 034338 (2022).

[14] A. N. Andreyev, S. Antalic, D. Ackermann, T. E. Cocolios, V. F. Comas, J. Elseviers, S. Franchoo, S. Heinz, J. A. Heredia, F. P. Heßberger, *et al.*, Phys. Rev. C **80**, 024302 (2009).

[15] A. N. Andreyev, D. Ackermann, F. P. Heßberger, S. Hofmann, M. Huyse, I. Kojouharov, B. Kindler, B. Lommel, G. Münzenberg, R. D. Page, *et al.*, Eur. Phys. J. A **18**, 55 (2003).

[16] A. E. Barzakh, A. N. Andreyev, T. E. Cocolios, R. P. de Groote, D. V. Fedorov, V. N. Fedosseev, R. Ferrer, D. A. Fink, L. Ghys, M. Huyse, *et al.*, Phys. Rev. C **95**, 014324 (2017).

[17] A. N. Andreyev, D. Ackermann, S. Antalic, H. J. Boardman, P. Cagarda, J. Gerl, F. P. Heßberger, S. Hofmann, M. Huyse, D. Karlgren, *et al.*, Eur. Phys. J. A **18**, 39 (2003).

[18] A. E. Barzakh, L. K. Batist, D. V. Fedorov, V. S. Ivanov, K. A. Mezilev, P. L. Molkanov, F. V. Moroz, S. Y. Orlov, V. N. Panteleev, and Y. M. Volkov, Phys. Rev. C **88**, 024315 (2013).

[19] J. Gerl, K. Vijay Sai, M. Sainath, R. Gowrishankar, and K. Venkataramaniah, At. Data Nucl. Data Tables **94**, 701 (2008).

[20] F. Kondev, M. Carpenter, R. Janssens, K. Abu Saleem, I. Ahmad, H. Amro, J. Cizewski, M. Danchev, C. Davids, D. Hartley, *et al.*, Phys. Lett. B **512**, 268 (2001).

[21] R. Bark, S. Törmänen, T. Bäck, B. Cederwall, S. Ødegård, J. Cocks, K. Helariutta, P. Jones, R. Julin, S. Juutinen, *et al.*, Nucl. Phys. A **657**, 113 (1999).

[22] D. T. Joss, J. Simpson, E. S. Paul, R. D. Page, N. Amzal, D. E. Appelbe, T. Bäck, B. Cederwall, J. F. C. Cocks, D. M. Cullen, *et al.*, Phys. Rev. C **68**, 014303 (2003).

[23] Evaluated nuclear structure data file (ensdf), accessed 15 december 2024. http://www.nndc.bnl.gov/, .

[24] Z. Y. Zhang, L. Ma, Z. G. Gan, M. H. Huang, T. H. Huang, G. S. Li, X. L. Wu, G. B. Jia, L. Yu, H. B. Yang, *et al.*, Nucl. Instrum. Methods Phys. Res. B **317**, 315 (2013).

[25] H. Huang, H. Y. Wu, C. Y. Guo, W. Q. Zhang, Q. B. Zeng, D. X. Wang, Z. Liu, Z. H. Li, A. N. Andreyev, S. Antalic, *et al.*, Phys. Rev. C **110**, 014326 (2024).

[26] D. W. Luo, C. Y. Guo, S. Y. Zhang, Z. X. Zhou, D. X. Wang, H. Wu, Z. Li, H. Hua, L. Ni, J. Zhang, *et al.*, Nucl. Instrum. Methods Phys. Res. A **1075**, 170333 (2025).

[27] H. Y. Wu, Z. H. Li, H. Tan, H. Hua, J. Li, W. Hennig, W. K. Warburton, D. W. Luo, X. Wang, X. Q. Li, *et al.*, Nucl. Instrum. Methods Phys. Res. A **975**, 164200 (2020).

[28] R. Brun, F. Rademakers, *et al.*, Nucl. Instrum. Methods Phys. Res. A **389**, 81 (1997).

[29] P. M. Raddon, D. G. Jenkins, C. D. O'Leary, A. J. Simons, R. Wadsworth, A. N. Andreyev, R. D. Page, M. P. Carpenter, F. G. Kondev, T. Enqvist, *et al.*, Phys. Rev. C **70**, 064308 (2004).

[30] C. M. Baglin *et al.*, Nucl. Data Sheets **134**, 149 (2016).

[31] K.-H. Schmidt, C.-C. Sahm, K. Pielenz, and H.-G. Clerc, Z. Phys. A **316**, 19 (1984).

[32] X. Wang, Z. H. Li, Z. Liu, J. Li, H. Hua, H. Y. Lu, W. Q. Zhang, T. H. Huang, M. D. Sun, J. G. Wang, *et al.*, Nucl. Instrum. Methods Phys. Res. A **971**, 164068 (2020).

[33] R. Grzywacz, C. J. Gross, A. Korgul, S. N. Liddick, C. Mazzocchi, R. D. Page, K. Rykaczewski, *et al.*, Nucl. Instrum. Methods Phys. Res. B **261**, 1103 (2007).

[34] M. Karny, R. K. Grzywacz, J. C. Batchelder, C. R. Bingham, C. J. Gross, K. Hagino, J. H. Hamilton, Z. Janas, W. D. Kulp, J. W. McConnell, *et al.*, Phys. Rev. Lett. **90**, 012502 (2003).

[35] Y. Xiao, S. Go, R. Grzywacz, R. Orlandi, A. N. Andreyev, M. Asai, M. A. Bentley, G. de Angelis, C. J. Gross, P. Hausladen, *et al.*, Phys. Rev. C **100**, 034315 (2019).

[36] S. Agostinelli, J. Allison, K. Amako, J. Apostolakis, H. Araujo, P. Arce, M. Asai, D. Axen, S. Banerjee, G. Barrand, *et al.*, Nucl. Instrum. Methods Phys. Res. A **506**, 250 (2003).

[37] T. Kibédi, T. W. Burrows, M. B. Trzhaskovskaya, P. M. Davidson, C. W. Nestor, *et al.*, Nucl. Instrum. Methods Phys. Res. A **589**, 202 (2008).

[38] R. B. Firestone *et al.*, *Table of Isotopes: 1999 Update, 8th Edition* (Coral M. Baglin, S. Y. Frank Chu, 1999).

[39] A. N. Andreyev, K. Van de Vel, A. Barzakh, A. De Smet, H. De Witte, D. V. Fedorov, V. N. Fedoseyev, S. Franchoo, M. Górska, M. Huyse, *et al.*, Eur. Phys. J. A **14**, 63 (2002).

[40] S.-C. Wu *et al.*, Nucl. Data Sheets **106**, 367 (2005).

[41] M. Basunia *et al.*, Nucl. Data Sheets **110**, 999 (2009).

[42] X. Huang, M. Kang, *et al.*, Nucl. Data Sheets **121**, 395 (2014).

[43] X. Huang, C. Zhou, *et al.*, Nucl. Data Sheets **104**, 283 (2005).

[44] F. G. Kondev *et al.*, Nucl. Data Sheets **187**, 355 (2023).

[45] M. P. Carpenter, F. G. Kondev, R. V. F. Janssens, *et al.*, J. Phys. G **31**, S1599 (2005).

[46] J. O. Rasmussen *et al.*, Phys. Rev. **113**, 1593 (1959).

[47] B. R. Mottelson, S. G. Nilsson, *et al.*, Phys. Rev. **99**, 1615 (1955).

[48] S.-C. Wu *et al.*, Nucl. Data Sheets **106**, 619 (2005).

[49] T. Johnson, B. Singh, *et al.*, Nucl. Data Sheets **142**, 1 (2017).

[50] M. Basunia *et al.*, Nucl. Data Sheets **195**, 368 (2024).

[51] M. S. Basunia *et al.*, Nucl. Data Sheets **143**, 1 (2017).

[52] B. Singh *et al.*, Nucl. Data Sheets **108**, 79 (2007).